JOURNAL OF THERMOPHYSICS AND HEAT TRANSFER
Vol. 10, No. 4, October–December 1996

Nose-Tip Surface Heat Reduction Mechanism

W. A. Engblom* and D. B. Goldstein†
University of Texas at Austin, Austin, Texas 78712

Hypersonic flow over the nose of a blunt body with a forward-facing cavity is examined. Strong resonant pressure oscillations within the cavity are a common experimental flow feature and occur numerically if either significant freestream fluctuations are present or a sufficiently deep cavity is employed. Substantial surface nose-tip cooling is achieved by creating strong longitudinal pressure oscillations within the cavity to induce large bow shock oscillations. Because of the motion of the bow shock relative to the body, the mean stagnation temperature of the airflow into the cavity is reduced. The cooling benefit increases with mean bow shock oscillation speed. Rounding the cavity lip is also necessary to reduce local surface heating since the airflow into the cavity directly impinges on the cavity lip.

Nomenclature

D = cavity diameter, cm
d = bow shock peak-to-peak displacement, mm
f_1 = primary mode frequency, Hz
G = pressure amplification at cavity base
L = cavity length or depth, cm
L^* = characteristic length, cm
$\bar{P}$ = mean base pressure, Pa
$P_{\text{base,rms}}$ = cavity base pressure rms
P_{t_2} = stagnation pressure behind normal shock, Pa
P_∞ = freestream static pressure, Pa
$P_{\infty,\text{rms}}$ = freestream static pressure rms
S_{shock} = average bow shock speed relative to body, m/s
T_i = initial surface temperature, K
T_0 = steady flow stagnation temperature, K
y^+ = local thickness Reynolds number
δ = bow shock standoff distance, mm
ρ_∞ = freestream density, kg/m^3
τ = oscillation period, s

I. Introduction

HYPERSONIC vehicles are designed to withstand severe heat loads. Such vehicles include hypervelocity projectiles, interceptor missiles, re-entry vehicles, and hypersonic aircraft. Maximum heating and, hence, the potential for material ablation, is typically most critical at the nose tip.

Of particular interest, hypervelocity projectiles can have large penetration depths[1,2] into armor because of their very high kinetic energy at impact, and consequently, the U.S. Army is interested in their development. However, in the flight regime 2–4 km/s, the projectile nose experiences high heating rates and ablation can produce unacceptable perturbations in the aerodynamics and the flight path. As an example of the severity of the heating, the stagnation temperature at sea level and a velocity of about 3.1 km/s (Mach 8.9) corresponds to the melting point of tungsten. There is therefore a need to develop active or passive techniques to reduce tip heating rates.

There has been speculation that introducing an axial cavity in the blunt nose region of a hypersonic vehicle (Fig. 1) may reduce peak heating during flight. The objective of this study is to determine if and how surface heating rates are affected by the presence of the cavity. The results presented herein include strong numerical and experimental evidence of a newly discovered surface heat reduction mechanism.

II. Background

Hartmann[3] introduced a new technique for producing sound of high intensity and discrete frequency known as the Hartmann whistle concept. This concept involves the flow of a supersonic jet over a body containing a forward-facing cavity. Research efforts related to these ideas (through the early 1960s) have been reviewed.[4]

It was reported[5] more than 30 years ago that the stagnation point heat transfer rate for a concave axisymmetric nose cone at supersonic Mach numbers is considerably lower than that of a convex nose cone. More recently, Huebner and Utreja[6] have shown that for a nose/cavity configuration the heat transfer rate at the cavity base, where convection is weak, is less than that at the rim of the nose.

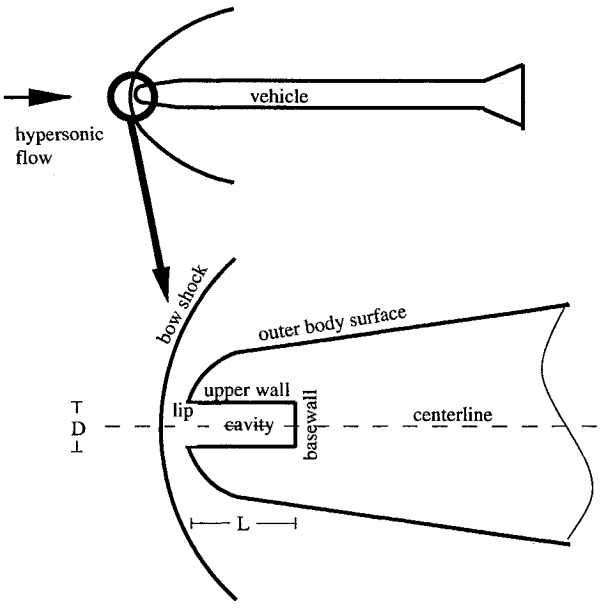

Fig. 1 Schematic of axial cavity in the nose region of a hypersonic vehicle.

Presented as Paper 96-0354 at the AIAA 34th Aerospace Sciences Meeting and Exhibit, Reno, NV, Jan. 15–18, 1996; received Jan. 29, 1996; revision received May 15, 1996; accepted for publication May 15, 1996.

*Graduate Research Assistant, Center for Aeromechanics Research, Department of Aerospace Engineering and Engineering Mechanics. Student Member AIAA.

†Assistant Professor, Center for Aeromechanics Research, Department of Aerospace Engineering and Engineering Mechanics. Member AIAA.

Preliminary experiments using an infrared (IR) camera by Yuceil et al.[7] indicated that larger diameter, shallow cavities [length-to-diameter (L/D) between 0.15–0.35] created a stable cool ring just outside of a sharp cavity lip with temperatures locally lower than those of a simple spherical nose.

A joint numerical and experimental effort by Engblom et al.[8] concluded that sharp cavity lips produce a separated recirculation region (which accounts for the cool ring), and severe heating just inside the cavity for weakly oscillating flows. Rounding the lip alleviates heating inside the cavity. Experimental results showed that the strong oscillations associated with deep cavities may provide an additional cooling effect.

III. Methodology

This article presents results from a numerical study. Experimental results are referenced to further substantiate important conclusions.

A. Computer Code Description

The commercial code INCA[9] (licensed from Amtec Engineering) was used for this study. INCA is a finite volume code that utilizes flux splitting with upwinding to capture strong shocks. Fluxes are computed with the flux splitting of Steger and Warming.[10] INCA offers an efficient LU–SGS (lower–upper successive Gauss–Seidel) implicit solver to calculate steady flowfields. The LU–SGS algorithm approximately solves the system of equations using two sweeps of a point Gauss–Seidel relaxation. INCA offers a variation of the LU–SGS implicit solver to calculate unsteady flows. This algorithm permits much larger time steps than a simple Euler step by performing a sufficient number of subiterations at each time step. This algorithm is also second-order accurate in time and space. All grid generation is performed using GRIDALL (Ref. 9). GRIDALL is capable of producing orthogonal grids based on the solution to the Laplace equation with boundary constraints.

B. Numerical Assumptions

The numerical model is a hemispherically blunted cylinder, 5.08 cm in diameter, with an axial cavity of length L from the base to the lip (similar to Fig. 1). The cavity diameter D is 2.54 cm. The cavity lip is modeled as either sharp (0.1-mm lip radius) or rounded (1.0-mm lip radius). However, in certain cases the sharp lip is modeled as infinitely sharp. These configurations correspond directly with similar experimental models being tested in the Mach 5 blowdown wind tunnel at the University of Texas at Austin.[8] The baseline case for both computations and experiments is a hemisphere–cylinder body without a cavity (i.e., $L/D = 0$).

The computational freestream conditions also correspond to those in the Mach 5 blowdown facility. Specifically, the freestream temperature and pressure are 64 K and 4694 Pa, respectively. Numerical simulation of freestream noise in the wind tunnel is discussed in Sec. IV.

Several simplifying assumptions are made in the simulations. The flow is assumed axisymmetric. This is appropriate because pressure oscillations at the cavity base in experiments[8] are typically planar (i.e., negligible radial variations). Because of the small scale of the flowfield (i.e., nose region) the flow is assumed laminar. The freestream Reynolds number is roughly 5.0×10^5/cm. The actual Reynolds number (per centimeter) is much smaller along the body surface inside the cavity because of the low speed of the flow. Since the characteristic flow lengths are less than 1 cm and a favorable pressure gradient is present, transition is not expected to occur within the cavity unless the oscillations within the cavity cause the flow to trip. An isothermal wall constraint ($T_{wall} = 300$ K) is used when surface heat rates are of interest. The adiabatic wall constraint eliminates wall heat conduction effects and permits the study of unsteady convection and viscous dissipation effects on the mean temperature field. The minimum and maximum flow temperatures in the simulations presented herein always remain within 64 and 530 K. Since the specific heats change less than 5% over this temperature range, the flow is assumed calorically perfect.

C. Numerical Procedure

Steady flowfield results are obtained via the implicit LU–SGS algorithm. Heat flux estimates for steady flowfields are obtained with a relatively fine grid near the body surface. A surface cell thickness of 1.0×10^{-3} mm is chosen for the sharp lip radius (0.1 mm) and rounded lip radius (1.0 mm) cavity configurations. This cell thickness was determined from a grid refinement study to allow for sufficient accuracy of the steady flow, surface heat flux distributions. However, severe peak heat values near the sharp lip could not be resolved precisely and should be considered rough estimates. A surface cell thickness of 2.5×10^{-3} mm is chosen for the infinitely sharp lip cases. This fineness is sufficient to resolve the surface heat flux except for the lip region. A moderately fine grid is also needed to resolve the bow shock (0.2-mm cell thickness).

Time-accurate unsteady simulations are conducted using the LU–SGS method with subiterations. The surface heat flux data from 100 realizations (points in time) during each cycle are averaged to obtain the mean surface heat flux distribution. This mean distribution is insensitive to the number of realizations if 50 or more are used. The solution is considered pseudosteady when the mean surface heat flux distribution does not change from one cycle to the next. Note, pressure oscillations within the cavity typically become pseudosteady (i.e., repeatable) well before the mean surface heat flux.

A grid refinement study is performed for each case in which surface heating is important. Specifically, the grid fineness level near the wall is increased by constant factors until grid independence of the mean surface heat flux distribution is obtained. A typical fine-grid solution includes a surface cell thickness of 1.0×10^{-3} mm, which corresponds to a maximum mean y^+ value of approximately 0.5 near the cavity lip. For cases involving an infinitely sharp lip the refinement study must exclude the lip region. Further details regarding grids are provided in Sec. IV.

The sensitivity of the residual (the measure of convergence level) to the global time step and number of subiterations are studied for each case. This study ensures temporal convergence and helps to determine which parameters provide the most efficient solution (minimum cost). Generally, one cavity oscillation (cycle) is solved using between 10^3–10^4 global time steps, and between 5–10 subiterations at each time step, depending on grid fineness and overall grid size. The corresponding CPU time requirement is about 0.5–10 h/cycle on a Cray Y-MP or 4–80 h/cycle on a DEC 3000/700.

IV. Results

Section IV.A provides a general description of a newly discovered surface heat reduction mechanism. Section IV.B includes numerical simulation data for a specific medium depth cavity ($L/D = 0.75$) case, which clearly illustrates the cooling mechanism. Section IV.C provides experimental and numerical data for a deep cavity ($L/D = 2.0$) case that further validates the cooling mechanism. Section IV.D provides limited numerical data for a very deep cavity case ($L/D = 5.0$) to prove that mean bow shock speed (not oscillation strength) is a key to substantial heat reduction. Section IV.E briefly addresses drag behavior.

A. Description of Cooling Mechanism

Oscillating pressure levels within a forward-facing cavity in hypersonic flow are a dominant experimental flow feature. Resonant frequencies are obtained by spectral analysis of the fluctuating pressure measurements made at the base of the cavity. Most of the energy of the oscillations is contained in the primary mode (i.e., quarter-wave or organ–pipe frequency).

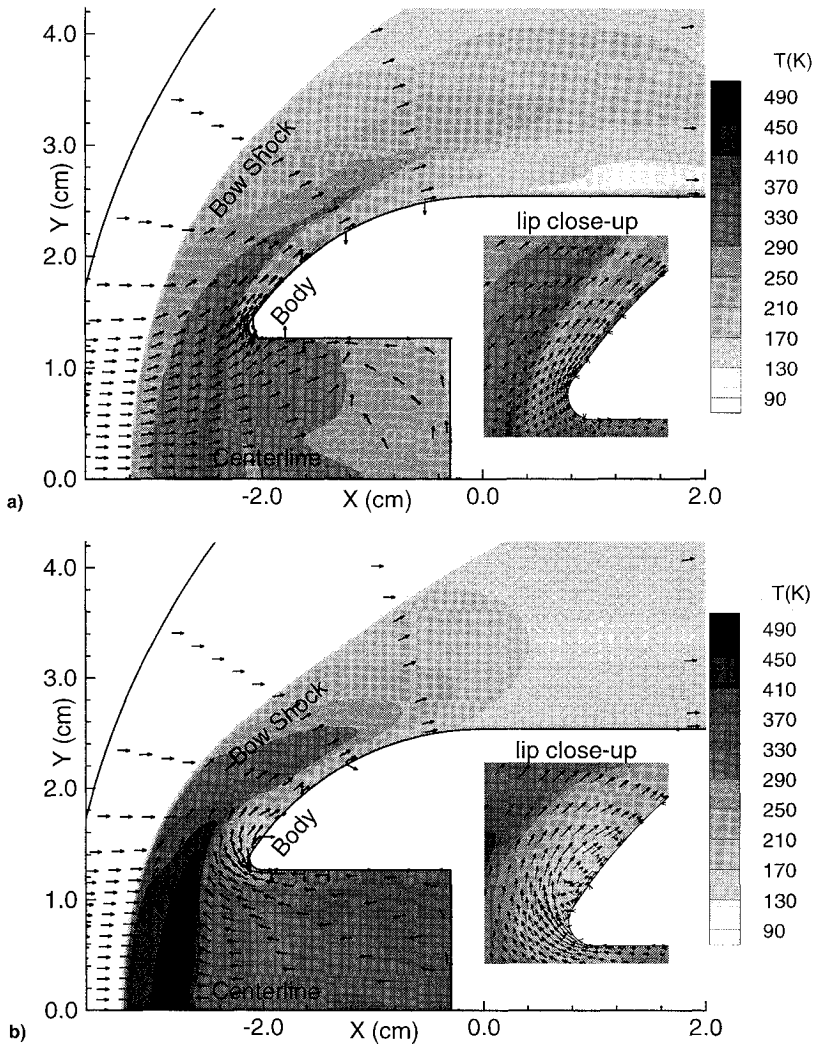

Fig. 2 Temperature contours (vectors on large plot indicate flow direction): a) cavity inflow, shock moving aft and b) cavity outflow, shock moving forward.

Time-accurate numerical simulations indicate that resonant oscillations are obtained if either freestream fluctuations are present (e.g., unsteady freestream pressure and density at the inflow boundary) or a sufficiently deep cavity is employed.[11] It may also be possible to force strong oscillations within the cavity by other means.

It has been discovered that the air flowing into the cavity is cooler than in a similar steady flow where no oscillations are present. Strong longitudinal pressure oscillations within the cavity correspond to strong longitudinal oscillations of the bow shock position. Typically the bow shock position oscillates almost sinusoidally between two positions: one relatively close to the cavity mouth and one relatively far upstream. During the inflow portion of the cycle the bow shock is moving toward the cavity mouth, thereby reducing the relative shock Mach number and the stagnation temperature of the inflow air. During the outflow portion of the cycle the bow shock is moving upstream, increasing the relative shock Mach number and the stagnation temperature of the inflow air. However, because of the cavity outflow, this hot air is convected away from the nose-tip region. Temperature contour plots illustrate the effect of bow shock motion during inflow (Fig. 2a) and outflow (Fig. 2b). Note that the air temperatures just downstream of the bow shock are much lower during the inflow phase. During outflow the flow also separates and forms a recirculation region that protects the outer surface from the extremely hot gas convecting away from the nose region. Consequently, the fluid mechanics of oscillating forward-facing cavity flow reduces the mean stagnation temperature of the flow in the vicinity of the nose tip and results in a net reduction in surface heating. Note, dramatic bow shock motion (i.e., large mean bow shock speed) is necessary to produce a substantial cooling effect. Quantitative results for several strongly oscillating cases are presented later.

B. Medium Depth Cavity Case

To clearly illustrate and validate the cooling mechanism it is useful to discuss a specific numerical simulation. Consider a medium depth cavity with a L/D ratio of 0.75 and a lip radius of 1.0 mm. The Mach number of the flow is 5. Numerical resonance is achieved by the input of sinusoidal freestream pressure and density perturbations (freestream temperature is held constant). A peak-to-peak amplitude of $\pm 0.10 P_\infty$ and $\pm 0.10\ \rho_\infty$, respectively, drives pressure oscillations within the cavity at a constant frequency of 3600 Hz. This frequency is nearly f_1 of the cavity that is calculated from Eq. (1) (Ref. 8).

$$f_1 = \sqrt{\gamma R T_0}/4L^* \tag{1}$$

This equation is derived from the one-dimensional wave equation in classic organ–pipe theory. The numerator is the speed of sound inside the cavity, assuming the gas temperature is approximately the stagnation temperature T_0 of the flow. The denominator is the characteristic wavelength that is four times

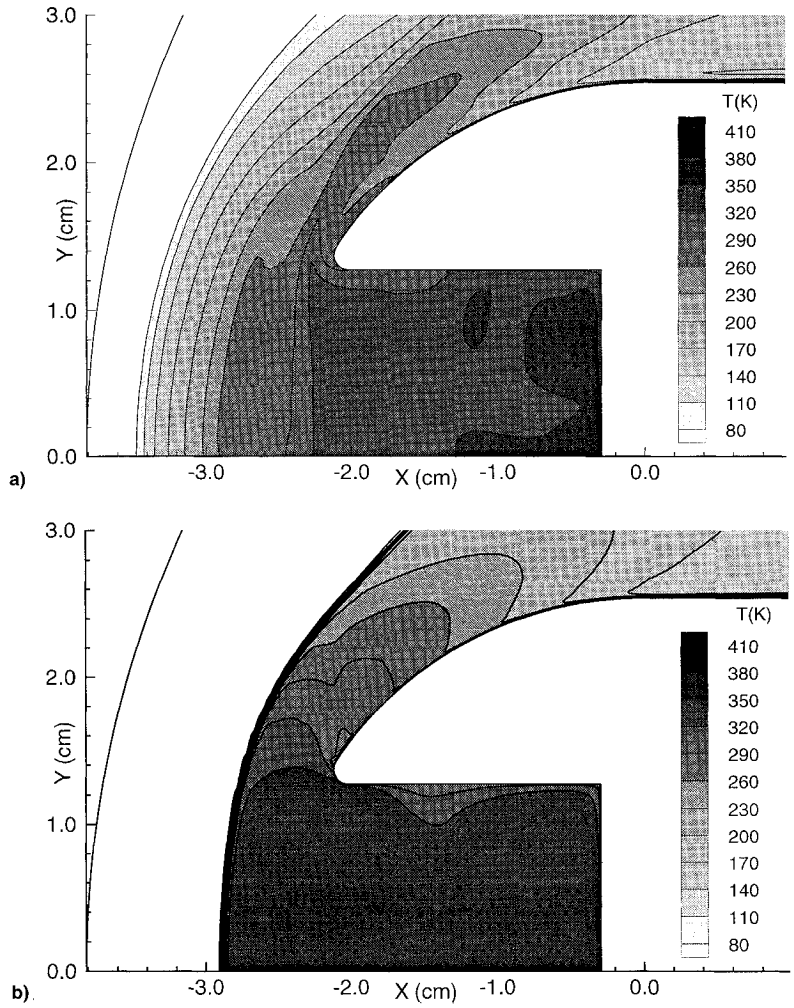

Fig. 3 Temperature contours (L/D = 0.75, 1.0-mm lip, 10% sinusoid): a) unsteady (mean) and b) steady flows.

the distance L^* between the mean bow shock location and the cavity base along the centerline.

These input waves result in large nearly sinusoidal stagnation pressure oscillations at the base of the cavity. The amplification G is defined as the ratio of the output (centerline base pressure) rms amplitude to the input (freestream) rms amplitude:

$$G = P_{\text{base,rms}}/P_{\infty,\text{rms}} \tag{2}$$

This case, driven with a perturbation input of $\pm 0.10 P_\infty$ and $\pm 0.10 \rho_\infty$ at 3600 Hz (7% rms), produces an output of approximately $\pm 0.42 P_{t_2}$ (30% rms) at 3600 Hz at the cavity base for an amplification $G = 4.2$. This perturbation input was selected to produce oscillations of similar strength to those produced in recent experiments.[8] For relatively shallow cavities (e.g., $L/D < 1.25$ at Mach 5) the oscillation strength and mean bow shock speed are directly proportional to the freestream perturbation rms level until saturation.[11] Without freestream perturbations this cavity geometry will not sustain oscillations. Note, atmospheric turbulence levels are generally not sufficient to produce strong pressure oscillations.

The unsteady pressure and temperature fields (but not the surface heat flux) are obtained with a relatively coarse grid along the body surface. A mean temperature contour plot (time-averaged over one cycle) for the strongly oscillating case is compared to a steady temperature contour plot (same cavity configuration without freestream perturbations) in Figs. 3a and 3b. There is clearly a substantial reduction in mean gas temperatures in the cavity and near the external surface as a result of the strong oscillations. The mechanism for this formation of a cool region was described in Sec. IV.A. For this case the mean bow shock speed is approximately 86 m/s.

The temperatures near the cavity base are similar in both the steady and unsteady contour plots because there is very little mean convection taking place. Although strong pressure oscillations at the cavity base correspond to significant temperature oscillations, the increase in heating during compression is approximately counteracted by the decrease in heating during expansion (nearly an adiabatic compression and expansion). The temperatures near the cavity base are virtually unchanged by a few oscillations. However, there might be a significant change in these temperatures over many cycles. After the initial transients have disappeared (3–5 cycles) the mean temperatures near the base of the cavity are approximately the steady flow stagnation temperature (370 K). Because of the cooling mechanism, however, we expect that the air flowing into the cavity is relatively cool compared to the steady flow stagnation temperature. Consequently, after many cycles this cool air may replace the hotter air within the cavity. Computational limitations restricted this simulation to a few dozen cycles and it has not been feasible to draw a definite conclusion. Results of an investigation of base heating for a different case are given in Sec. IV.C. Regardless, if cavity base heating were still a problem, it is possible to inject a small amount of cold gas into the cavity that will only be slowly convected away.

A grid refinement study is conducted to ensure convergence of the time-dependent surface heating. The five grids studied each contain 196 points along the body surface. This spatial resolution is adequate for fine resolution of steady flowfield features and is assumed adequate for the unsteady case. The

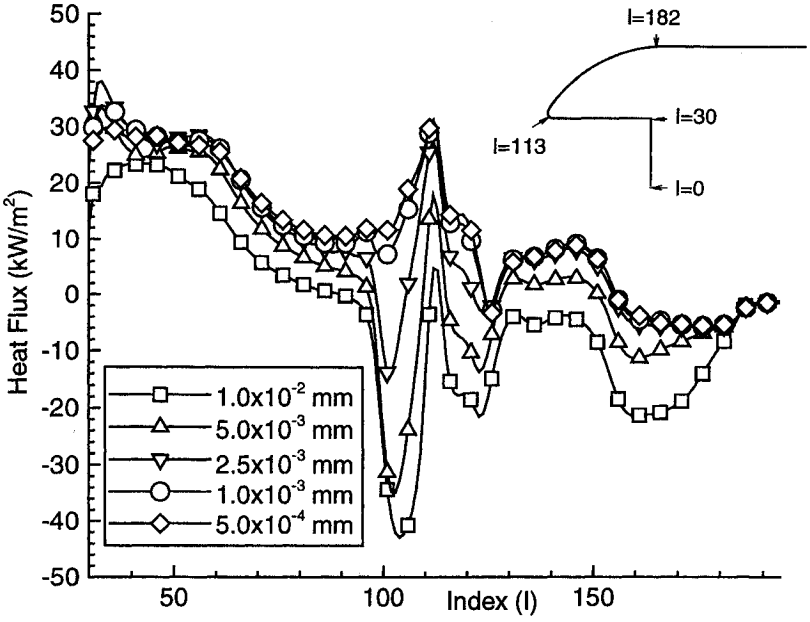

Fig. 4 Mean surface heat flux distribution for various surface grid fineness levels.

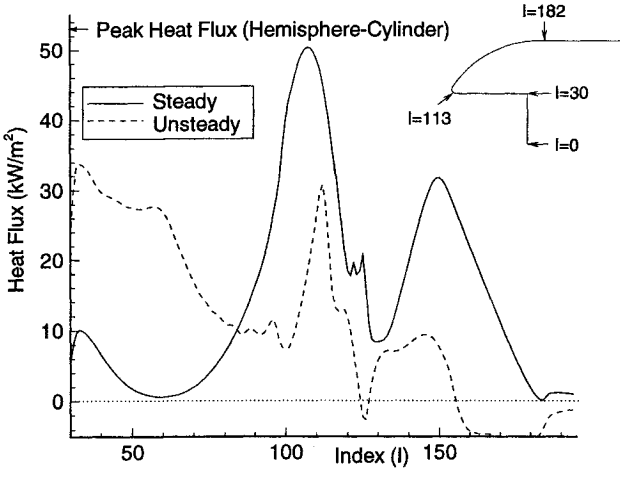

Fig. 5 Unsteady (mean) and steady heat flux distributions (round lip).

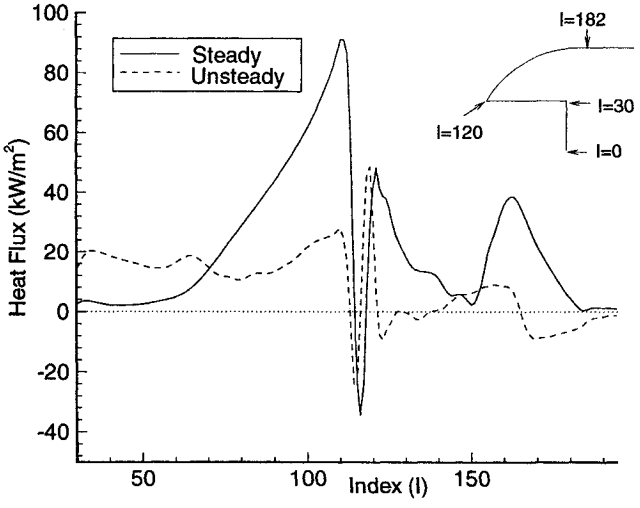

Fig. 6 Unsteady (mean) and steady heat flux distributions (sharp lip).

fineness level of the grid near the wall (i.e., surface cell thickness) varies among the five grids employed from 1.0×10^{-2} to 5.0×10^{-4} mm. The grids contain between 125–165 cells normal to the wall, depending on the grid fineness.

Mean surface heat flux distributions (averaged over one cycle) for each of the five grids are shown in Fig. 4. Note, the distributions are given as a function of I (index location) starting from the base of the cavity on the upper wall. The distribution along the base of the cavity is not included because the base heating is not considered completely pseudosteady (as discussed earlier). Sufficient convergence is obtained everywhere along the outer surface and cavity lip for the fine grid (1.0×10^{-3} mm surface cell thickness) as demonstrated by the coincidence of the 1.0×10^{-3} and 5.0×10^{-4} mm curves. Sufficient convergence is also obtained along the cavity upper wall since the distribution remains contained within a narrow band. This band reflects a slight unsteadiness of the surface heating inside the cavity that is largest near the cavity base. Comparison of the unsteady (mean) heat flux distribution with the steady heat flux distribution indicates a substantial cooling effect (Fig. 5). The peak heat flux for the baseline case (53 kW/m^2) is included as a reference value. The peak surface heating for the steady case (50 kW/m^2) occurs just inside the cavity, near the lip (I = 105) and at the reattachment location (I = 150).[8] The peak surface heating in the unsteady case (31 kW/m^2) occurs directly on the cavity lip (I = 113) because the air as it flows into the cavity impinges directly upon the cavity lip. The stagnation point remains at the cavity lip during most of the inflow phase. The peak heating associated with reattachment is dramatically reduced. Modest local hot spots exist near the base of the cavity along the upper wall (I = 30–60) since some of the hot gas formed during cavity outflow is convected into the cavity during the inflow phase. It appears likely that the cavity geometry or inflow conditions could be modified to reduce or eliminate these hot spots.

A similar analysis is performed for the same case except with a sharp lip (0.1 mm radius) to determine the sensitivity of peak unsteady heating to lip radius. Figure 6 provides a comparison of the unsteady surface heat flux distribution with the steady heat flux distribution for the sharp lip case. The peak surface heating for the steady case (90 kW/m^2) occurs just inside the cavity, near the lip (I = 110), and at the reattachment locations of the primary (I = 160) and secondary vortices (I = 122).[8] The peak unsteady heating is relatively large (51 kW/m^2) and again occurs directly on the cavity lip (I = 120). This increase is expected since the flow directly

impinges the sharp cavity lip. The peak heating associated with reattachment is dramatically reduced. Local hot spots near the cavity basewall are also observed in the simulations.

C. Deep Cavity Case

To further validate the cooling mechanism an experiment in which substantial cooling was reported is numerically emulated. Yuceil[12] reported results for a deep cavity with an L/D = 2.0 and a sharp lip (approximately 0.1-mm lip radius) in a Mach 5 blowdown tunnel. Temperature histories measured at a point just outside the lip are shown in Fig. 7 for the deep cavity and baseline cases. The surface temperature rise in time (taken as representative of the heat flux) is much slower for the deep cavity case. Note, IR temperature measurements take into account the surface emissivity, viewing angles, and resolution.

As mentioned earlier, time-accurate numerical simulations[11] indicate that relatively deep cavities will self-sustain large oscillations without the presence of freestream noise (i.e., deep cavities are unstable). For an L/D = 2.0 cavity case, the oscillations are almost the same strength, regardless of whether or not tunnel inflow noise is included in the simulation. Hence, this cavity produces self-sustaining oscillations.

The numerical freestream noise is estimated from the inflow noise level present during operation of the Mach 5 blowdown tunnel. Specifically, experimental measurements of the stagnation pressure for the baseline shape are rescaled to model the numerical freestream static pressure and density history. The experimental pressure signal had an rms deviation of approximately 1.15% P_{t_2} and a broadband spectrum.[8] The numerical freestream noise is modeled essentially as plane waves (one-dimensional waves with negligible radial variations) and involves variations in pressure and density only, whereas the experimental noise involves three-dimensional variations in all fluid variables.

The same body dimensions are used in the numerical simulation of the deep cavity case, except that the lip is infinitely sharp. This lip is modeled in this way because the grid is composed of two zones, one for the cavity interior (30 × 200) and one for everywhere else (80 × 80). Note, it is not possible to obtain an accurate surface heating estimate for the few grid points that form the numerical lip, since an infinitely sharp lip would encounter an infinite heat rate. Sensitivity studies have shown that the strength of bow shock oscillation and the resulting mean temperature field are virtually unchanged whether the lip is infinitely sharp or slightly rounded. Consequently, either type of grid can be used to determine if the cooling mechanism is present.

The simulation required approximately 100 oscillation cycles (0.067 s of real time) before reaching a reasonably pseudo-steady solution. Due to the presence of inflow noise the oscillations are not exactly periodic. The simulations are considered pseudosteady once the mean surface heat flux distribution and rms base pressure level do not change significantly for several consecutive cycles. The simulation is performed using a coarse grid until a pseudo-steady state is reached. Grid fineness is then increased by interpolation and the simulation continued until a fine grid mean surface heating distribution is obtained. A surface cell fineness of 2.5 × 10^{-3} mm is chosen based on a grid convergence study (excluding lip region).

A portion of the time-accurate results for the pressure history at the base of the cavity is presented in Fig. 8. The freestream noise input is also shown. These pressure histories have been normalized to indicate the percentage variation from the mean value. A detailed power spectrum of the simulation is difficult to obtain because of limited computer resources. However, it is clear that most of the energy of the oscillations is contained in a primary mode of approximately 1500 Hz in agreement with experiments. The rms deviation of the output base pressure is approximately 21%. The rms deviation of the output base pressure in the experiment is 32% (Ref. 12). Recent measurements of the experimental tunnel noise level estimate the noise rms at 1.37% (compared to the 1.15% implemented in the numerical simulation). The noise level has a minor effect on the oscillation strength and does not account for the significant difference between the experiment and numerics. Results from a spatial and temporal sensitivity study indicate this solution is numerically converged. Possible reasons for the discrepancy include numerical omission of three-dimensional effects, turbulence, and heat conduction or some unknown experimental effect.

A mean temperature contour plot (time averaged over one cycle) for the unsteady deep cavity case is compared to a steady flow temperature contour plot in Fig. 9. There is a modest reduction in the mean gas temperatures near the lip caused by the cooling mechanism. The mean (unsteady) temperature of the gas inside the cavity is higher than in the steady case because of the convection of hot gas (relative to the wall temperature). Note, the steady flow cavity gas temperatures approach the wall temperature (300 K) since the flow is essentially stagnant.

The mean surface heat flux distribution for the outer surface is compared to the steady heat flux distribution in Fig. 10. The heating associated with reattachment (along the outer surface) is alleviated. A modest reduction in the peak surface heating just inside the cavity, near the lip, is also achieved (not shown). It is expected that the cooling effect would be more significant if the base pressure rms levels and corresponding shock motion were stronger and more closely matched the experiment. The mean bow shock speed for this case is approximately 20 m/s.

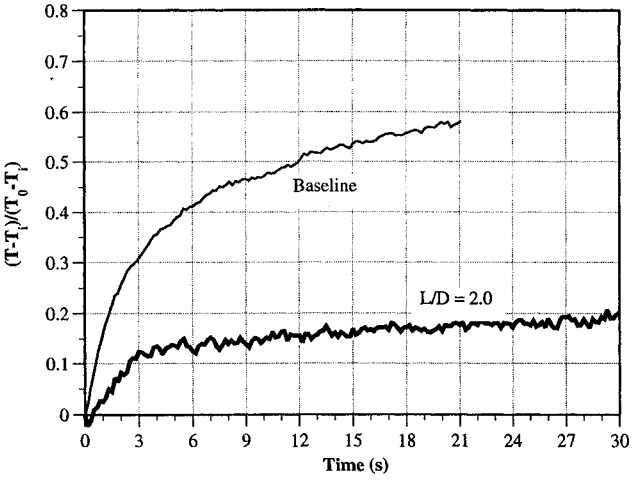

Fig. 7 Surface temperature histories (IR camera).

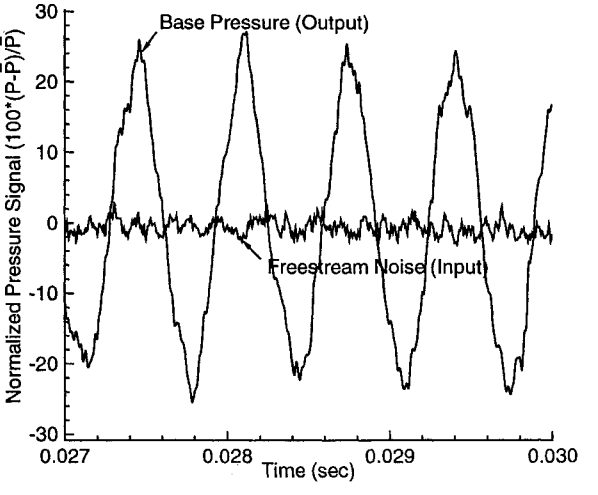

Fig. 8 Pressure history (L/D = 2.0).

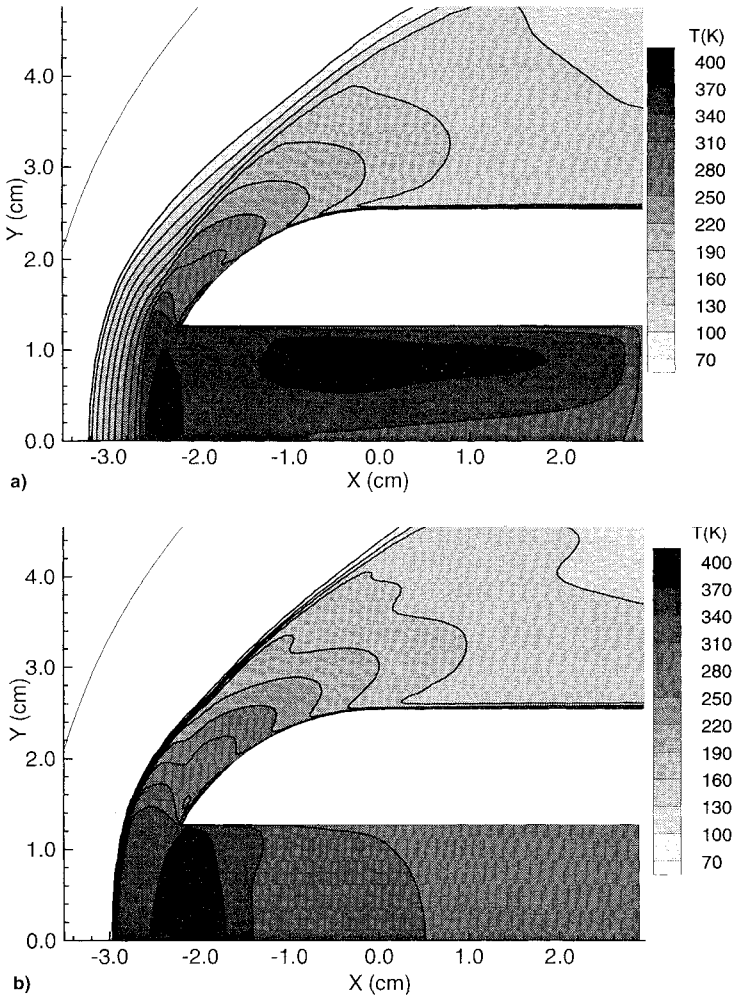

Fig. 9 Temperature contours (L/D = 2.0, isothermal wall): a) unsteady (mean) and b) steady flows.

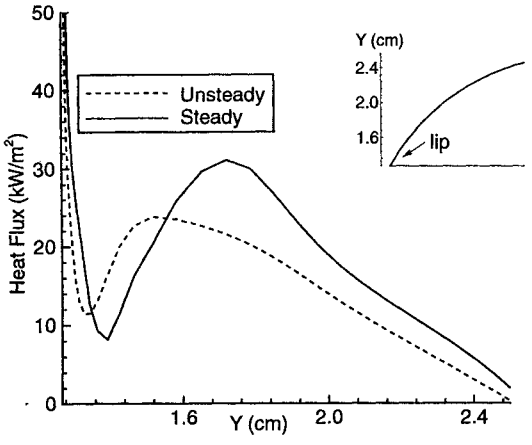

Fig. 10 Outer surface heat flux distributions (L/D = 2.0).

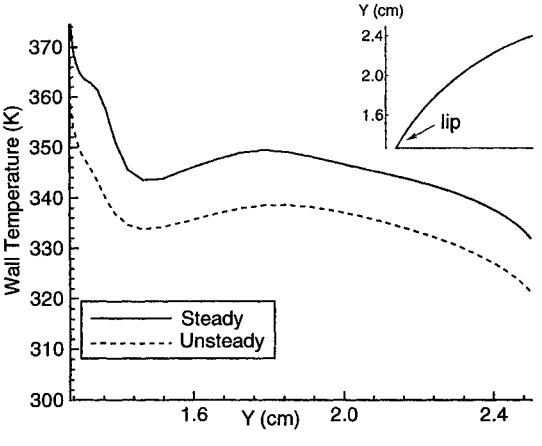

Fig. 11 Outer surface temperature distributions (L/D = 2.0).

The rise in heat flux along most of the cavity upper wall in the unsteady case is caused by convection, but results in relatively modest heating. Cavity basewall heat rates are negligible in the simulations (1–2 kW/m^2) after initial transients disappear because of extremely weak convection. The gas near the cavity basewall experiences nearly adiabatic gas compression/expansion.

A similar analysis is performed for the same case except with an adiabatic wall condition. The mean surface temperature distribution along the outer surface is compared to the steady temperature distribution in Fig. 11. A small reduction (3%) in surface temperatures is shown. The cavity basewall temperatures reach a maximum of 365 ± 2 K, which is slightly below the steady flow stagnation temperature of 371 K. This suggests that the mean air temperature of the gas flowing into the cavity is reduced by the cooling mechanism.

D. Very Deep Cavity Case

Numerical and experimental results indicate that the strength of oscillations (base pressure rms) increases with cavity depth, for otherwise fixed geometry and freestream conditions, and eventually plateaus or saturates.[11] Bow shock motion correspondingly plateaus. Specifically, during very strong oscillation the shock exhibits a bistable oscillation mode in which

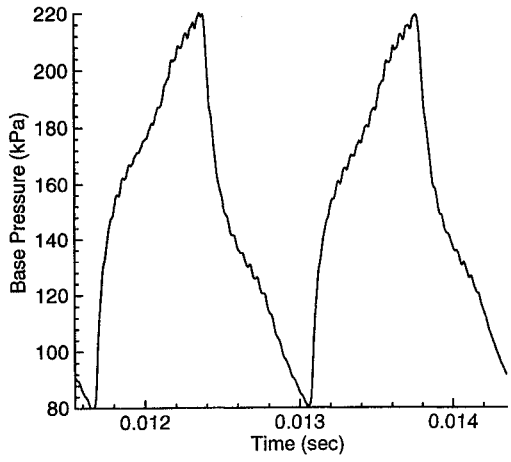

Fig. 12 Base pressure history (L/D = 5.0).

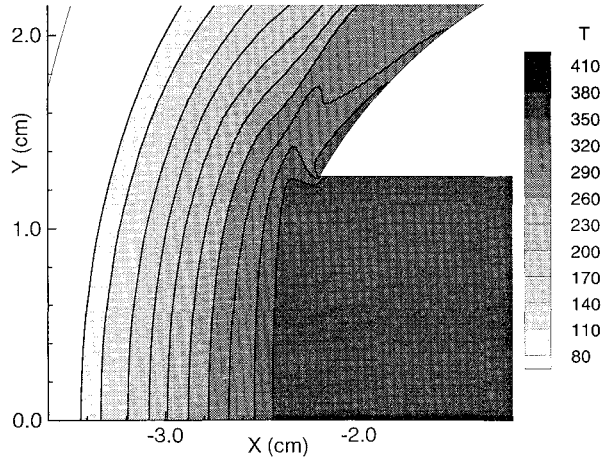

Fig. 13 Mean temperature contours near the cavity mouth (L/D = 5.0, adiabatic wall).

the shock is located at the maximum downstream position (the mouth of the cavity) or a maximum upstream position for a large portion of the oscillation period. The bow shock moves abruptly between these two locations. This bistable oscillation mode had been noted in early research on the Hartmann whistle.[4]

The maximum distance a bow shock can move downstream is δ. Correspondingly, d is limited to roughly 2δ. Note also that τ increases with cavity depth according to Eq. (1). Consequently, the average bow shock speed relative to the body S_{shock} must contain a maximum with cavity depth since

$$S_{\text{shock}} \approx 2d/\tau, \qquad d \leq 2\delta \tag{3}$$

For shallow cavities, oscillations are weak to nonexistent in quiet flow so that shock motion is small. For deep cavities shock displacements are large ($\sim 2\delta$), but the period is so long that, again, the mean shock speed is small. Shock velocity appears to be the key to substantial heat reduction. Consequently, there should be an optimum cavity depth that provides the maximum cooling benefit for otherwise fixed geometry and freestream conditions.

To further substantiate these observations a simulation is performed for a very deep cavity (L/D = 5.0). The freestream conditions are again simulating the Mach 5 blowdown tunnel, except without freestream noise. The grid is composed of two zones, one for the cavity interior (30 × 400) and one for everywhere else (80 × 80). Only a relatively coarse grid along the walls is required to obtain an accurate pressure history and mean temperature contour plot.

A base pressure history is shown in Fig. 12. The bistable motion of the shock is observed. This motion is implied by the shape of the base pressure history in which the pressure expansion and compression are abrupt. These pressure oscillations are very strong (27% rms variation) and are similar in strength to the medium depth cavity case discussed in Sec. IV.B.

Direct comparison of the mean temperature contour plot (Fig. 13) with a similar plot for the medium depth cavity case (Fig. 3a) indicates no substantial heat reduction near the lip for this very deep cavity case. The mean bow shock speed is approximately 16 m/s for the very deep cavity case based on the simulation. This confirms that mean shock speed, not oscillation strength, is a key to substantial heat reduction.

E. Drag Behavior

There is essentially no change in drag between the steady and unsteady cases for a given configuration (i.e., <1%), since the pressure load oscillates nearly symmetrically about the steady flow pressure load. The drag coefficient for the rounded-lip nose-cavity configurations and the baseline shape (hemisphere–cylinder) are virtually identical (C_D = 0.93). Surprisingly, the drag is reduced by 3% when comparing these values to the sharp-lip configurations (C_D = 0.90).

V. Summary

A newly discovered nose-tip surface heat reduction mechanism is described. Numerical and experimental results indicate that significant surface nose-tip cooling is achieved by creating strong longitudinal pressure oscillations within the cavity to induce large bow shock oscillations. Because of the motion of the bow shock relative to the body, the mean stagnation temperature of the airflow into the cavity is reduced. The heat reduction benefit appears to increase with mean bow shock speed. Strong resonant pressure oscillations are generated within the cavity if either significant freestream fluctuations are present or a sufficiently deep cavity is employed.

Acknowledgments

Funding was provided by the Institute for Advanced Technology, under Aeronautical Research Laboratory Contract DAAA21-93-C0101, monitored by William G. Reinecke. The authors are grateful to Cray Research, Inc., for use of the Cray Y-MP at the University of Texas, to NASA Ames Research Center for use of the NAS supercomputer center, to Scott Imlay of Amtec Engineering for providing technical assistance with the numerical simulations, and to K. Bulent Yuceil for providing experimental data.

References

[1]Hohler, V., and Stilp, A. J., "Long Rod Penetration Mechanics," *High Velocity Impact Mechanics*, edited by J. A. Zukas, 1st ed., Wiley, New York, 1990, pp. 321–404.

[2]Baker, J., and Williams, A., "Hypervelocity Penetration of Plate Targets by Rod-Like Projectiles," *International Journal of Impact Engineering*, Vol. 5, No. 1, 1987, pp. 101–110.

[3]Hartmann, J., and Troll B., "On a New Method for the Generation of Sound Waves," *Physical Review*, Vol. 20, 1922, pp. 719–727.

[4]Powell, A., and Smith, T. J., "Experiments Concerning the Hartmann Whistle," Univ. of California, Dept. of Engineering, Rept. 64-42, Los Angeles, CA, Sept. 1964.

[5]Burbank, P. B., and Stallings, R. L., "Heat-Transfer and Pressure Measurements on a Flat-Face Cylinder at a Mach Number Range of 2.49 to 4.44," NASA TMX-221, 1959.

[6]Huebner, L. D., and Utreja, L. R., "Experimental Flowfield Measurements of a Nose Cavity Configuration," Society of Automotive Engineers Paper 871880, Oct. 1987.

[7]Yuceil, B., Dolling, D. S., and Wilson, D., "A Preliminary Investigation of the Helmholtz Resonator Concept for Heat Flux Reduction," AIAA Paper 93-2742, July 1993.

[8]Engblom, W. A., Yuceil, B., Goldstein, D. B., and Dolling, D. S., "Hypersonic Forward-Facing Cavity Flow: An Experimental and Numerical Study," AIAA Paper 95-0293, Jan. 1995.

[9]Imlay, S. T., Roberts, D. W., and Soetrisno, M., "INCA User's Manual," Amtec Engineering, Inc., Version 1.1, Bellevue, WA, Nov. 1992.

[10]Steger, J. L., and Warming, R. F., "Flux Vector Splitting of the Inviscid Gasdynamic Equations with Applications to Finite-Difference Methods," *Journal of Computational Physics*, Vol. 40, No. 2, 1981, pp. 263–293.

[11]Engblom, W. A., Goldstein, D. B., Ladoon, D., and Schneider, S., "Fluid Dynamics of Forward-Facing Cavity Flow," AIAA Paper 96-0667, Jan. 1996.

[12]Yuceil, B., *An Experimental Investigation of a Forward-Facing Nose Cavity on a Blunt Body at Mach 5*, Ph.D. Dissertation, Univ. of Texas, Austin, TX, Dec. 1995, pp. 77–94, 123–132.